Harvesting Renewable Energies through Innovative Kinetic Honeycomb Architectural Facades: The Mathematical & CFD Modeling for Wind Turbine Design Optimization

by Pak Danny Mintorogo

Harvesting Renewable Energies through Innovative Kinetic Honeycomb Architectural Facades:
The Mathematical & CFD Modeling for Wind Turbine Design Optimization

Abstract

The research was specifically focused on the renewable energy factors associated with thousands of hexagonal micro-module wind turbines, hexagonal solar cell modules, and hexagonal modules for solar-reflecting pipes. This involved the utilization of windmills and solar cells specifically designed in a non-structural facade of the front building envelope through a double facade technique. Moreover, electrical energy was obtained from each windmill module while extra renewable electricity from abundant sunlight was acquired through the hexagonal modules of the solar cells (photovoltaic) designed vertically on the building facade. But this current research only focuses on hexagonal wind turbines. ANSYS Fluent 12.0 simulated software and numerical analysis were used to optimize and redesign the wind turbine blades in order to obtain more electricity from one micro-module hexagonal wind turbine. The results showed that this design was able to produce 2.66 Watts per wind turbine compared to the 0.12 Watt from the previous design. The TSR was also found to be 0.5 and its power coefficient value (C_P) of 0.4525 was observed to be much higher than the 0.0343 from the previous design. Therefore, means multilevel buildings have the ability to harvest sustainable greenery energies from such a smart architectural façade.

Keywords: Harvest renewable energy; kinetic honeycomb architectural façade; numerical and simulated CFD; wind turbines design for second façade architecture buildings.

1. Introduction

The world has been experiencing an extreme global energy crisis since 1979 due to the high need for energy (Manieniyen, 2009). Several countries have, therefore, been exploiting conservative biomass such as fossil fuels in the form of gasoline, coal, oil, propane, and natural gas. According to the United States Energy Information Administration (EIA), un-canopies natural energies are usually used and these include 80% from fossil fuels as indicated by 35,3% petroleum, 19,6% coal, and 26,6% natural gas while only 8,3% is from nuclear energy, and 9.1% from renewable energy (Coyle, 2014, p.15). Moreover, nuclear reactors currently use uranium (U), plutonium (Pu), and thorium (Th) as fuel to produce energy. This led to the search for eco-friendly environmental energies from hydrogen as the alternative gasoline in order to reduce CO2 pollution and asthma prevalence. There are other eco-friendly energy sources except hydro-energy and nuclear power and these include solar power or photovoltaics which involves using the abundant sun rays through solar radiation to generate electricity. The process involves installing either fixed or rotatable solar panels for approximately 10 hours on rooftops, canopies, or facades. Another alternative is the force-moving kinetic wind or wind turbines which generate electricity silently for almost 24 hours (Dudley, 2008, p.39). Biomass is another option through direct heating or biomass boilers and involves burning urban dry leaves or pruned trees as well as house and farm unused papers to generate energy while increasing household incomes and reducing city garbage (Nowak et al., 2019).

Renewable energies are becoming more important in cities and rural areas due to the high demand for energy in recent decades for residential and commercial purposes, especially in remote areas such as islands located very far from government power plants (Daryanto, 2007). Previous studies showed that 31% of energy is consumed through transportation while residential and commercial buildings use nearly 40%-42% (Cao, Xilei & Liu, 2016) and have the greatest total essential energy consumed in the U.S. and E.U (EIA, 2004b). Moreover, the Energy Efficiency Division of the Philippines Department of Energy (DOE) (2002) showed that 15 to 20% of the total national energy in the country was consumed by buildings and industries while a higher percentage of 66% was reported in California, USA (California Energy Commission, 2005). It was also predicted that the energy needed by this sector from different sources in countries which are not members of the Organization for Economic Cooperation and Development Countries (OECD) between 2010 to 2050 is expected to increase from 50 quadrillions BTU to

approximately 32 - 82 quadrillion BTU while the value required by OECD members is expected to be from 7 quadrillions BTU to approximately 48 to 55 quadrillion BTU as indicated in Figure 1.
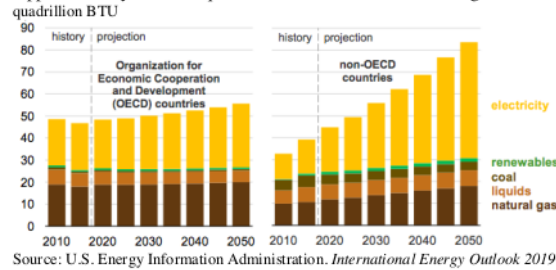

Source: U.S. Energy Information Administration. *International Energy Outlook 2019*
Figure 1. Energy Consumption in Buildings by Many Energy Resources (2010-2050)

This means more renewable energy is needed to generate and harvest sustainable electricity for residential and commercial or rental office buildings considering the small quantity it presently contributes when compared to the normal fossil oil as indicated in Figure 1. Countries of the world are observed to be constructing and consuming renewable energy, especially from solar and wind sources, as indicated by the annual average increase of 3.6% from 2018 to 2050 and a gradual decrease in coal-based energy consumption from 35% in 2018 to 22% at the end of 2050. This means coal is the current primary source while renewable energy is projected to contribute 50% of the total world electricity production in 2050 (International Energy Outlook, 2019). It is also important to note that Building Integrated Photovoltaics System (BIPV) through thousands of solar cells has also been installed across the world from 2013 to 2019 to generate around 5.4 GW and annual growth of 18.7% (Attoye, 2018).

The objective of this research was to propose and obtain renewable energies on building facades using honeycomb module wind turbines.
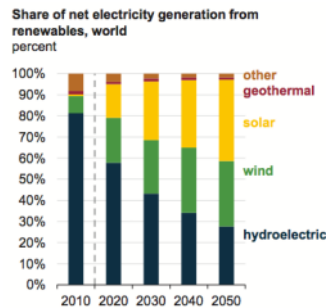

Source: U.S. Energy Information Administration. *International Energy Outlook 2019*
Figure 2. World Net Electricity Production from Renewable Sources (2010-2050)

2. Renewable Energy

The focus of this research is on renewable energy from solar and wind sources using a smart energy honeycomb façade. This façade depends on a double skin façade which has three parts which include the upper-part hexagonal module in the form of series of horizontal light pipes built on room ceilings to tap energy from daylight. The middle-part honeycomb module façades consist of thousands of micro-wind turbines to tap energy from kinetic wind sources while the bottom-part hexagonal modules include

2

thousands of photovoltaic cells used to harness energy from solar radiation as indicated in Figures 3A and B.
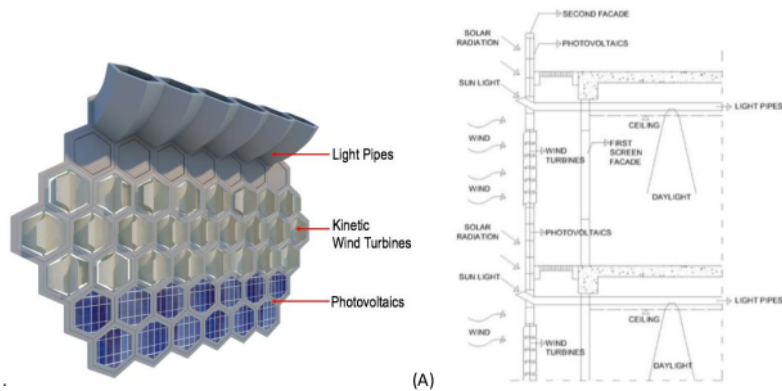

Figure 3. (A) Conceptual Double Skin Smart Façade (Light-Pipes, Wind Turbines, Photovoltaic Cells). (B) Schematic Building Section-Drawing showing features of light pipes, wind turbines, and photovoltaics.

2.1. Biomimicry Smart Façade Concept

The common double facade building technique applied has been reported to be very effective for energy conservation for a long period (Ahmed, 2016). It is also designed to save energy and assist in the process of collecting renewable energies as a contribution to finding solutions to the world energy crisis. Moreover, the idea of using the honeycomb form or bio-mimicry was based on the (1) regular modular to represent the rigidity of the facade structure and 2) each hexagon module is filled with honey which serves as the source of life for children of bees known as larvae and the queen bees as indicated in Figure 4A. This design is projected to retrieve renewable electricity using thousands of small windmills placed in one-third of the smart facade as shown in Figure 4B while solar cells are on the lower part and the hexagon-shaped reflection pipes are at the top as indicated in Figure 3A.
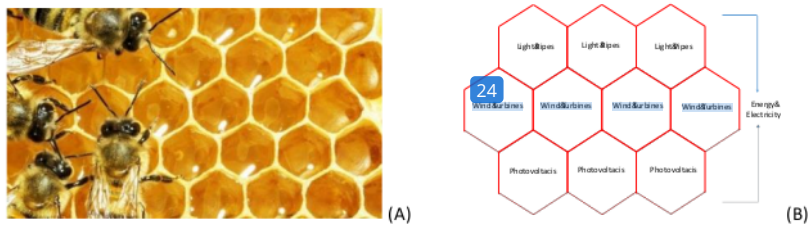

Figure 4. (A) Honeycomb, bees, and honey and (B) Honeycomb smart façade module and electricity

The term BIPV (Building Integrated Photovoltaic) is normally used to define buildings incorporated with PV circuits on the roof or envelope system. IBIPV systems can be used to replace roofing, curtain walls, glazing, or special elements such as eaves or canopies. It is usually applied in the concept of

green architecture as an energy-saving strategy through the utilization of solar radiation which is an environmentally friendly renewable energy source (Howells & Roehrl, 2012). Meanwhile, Building Integrated Wind Turbine (BIWT) is a building designed using wind turbines in the facades to produce energy (Arteaga-López, Ángeles-Camacho, & Bañuelos-Ruedas, 2019).

2.2. Renewable Wind Turbines Energy Systems

An example of renewable energy from wind is the windmill which can be divided into horizontal and vertical types. These two types have the same mechanism and this involves the wind moving the propeller which later drives the motor to produce electrical energy but the difference is observed from the placement of the quite heavy motor. It is, however, important to note that the vertical type is more advantageous due to its ability to match the weight of gravity which is straight down. Moreover, the movement of the propeller on the wind turbine due to kinetic energy as the wind pushes its surface depends on its horizontal or vertical placement. This classification was also observed in the rotation of the shaft as indicated by the one rotating vertically when the rotor is located in a horizontal position as well as the horizontal rotation when the rotor was placed vertically which has been further developed into Savonius, Darrieus, and H-Rotor as indicated in Figure 5A.
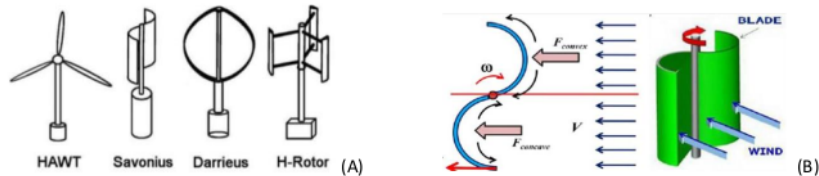
Figure 5. Horizontal and Vertical Rotating Propeller Placement (A)
Principles of Wind Turbine Movement in the Savonius System (B)

The wind turbine spins due to the difference in pressure on each blade. For example, one of the sunken sides of the Savonius vertical wind turbine captures the wind and spins it while the other side of the convex receives also wind and causes the turbine to spin as shown in Figure 5B (Wenehenubun, Saputra, & Sutanto, 2015). It is possible to turn the wind turbines in tall buildings over using two systems. The first involves using several large wind turbines placed on the roof of a building, between two adjacent buildings, or in a hole created inside the building as indicated in Figure 6A and this design can be found in the World Trade Center building in Bahrain. The second method is using many small wind turbines installed on buildings as showed in Figure 6B and this is considered advantageous due to the fact that the size of the turbines reduces its ability to overload the building structure but requires to be installed in high number to produce the energy needed. An example of these 2 designs can be found in the Miami Coral Tower in Miami (Park, Jung, Lee, & Park, 2015). Meanwhile, Savonius VAWT (S-VAWT) is a good candidate due to its high initial torque, low cost, easy installation and repair, and sturdiness (Manwell et al., 2010, 1-3).
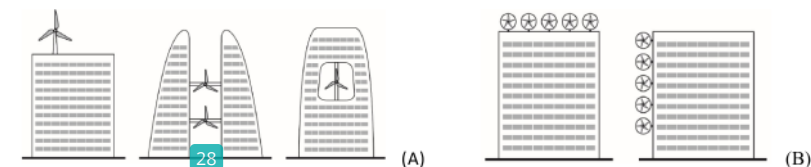
Figure 6. (A) Three Building Integrated Wind Turbine (BIWT) Systems using Large Wind Turbines and (B) Two BIWT Systems Use Small Sized Wind Turbines. (Source: Park, 2015).

4

3. Methodology Overview

The purpose of this research was to obtain the maximal values of electrical power from wind turbines' hexagonal frame smart façade module. It was focused on redesigning the wind turbine blades numerically after which they were simulated using ANSYS Fluent which is a simulation computational fluid dynamic (CFD) analysis program.

The previous experimental design of the Savonius wind turbine with 4 blades was used as the basis for the experimental model tested in the wind tunnel at the Mechanical Engineering laboratory and the Cp was found to be only 0.003426. Meanwhile, one module of hexagonal windmill produced 2.30 Volts, 0.05 Ampere, and 0.1182 Watt when the wind speed was 4 m/s while the values were 3.39 Volts, 0.01 Amperes, and 0.0607 Watt at 5 m/s (Mintorogo, 2019).

3.1. Shape and Size of Integrated Windmills in the Building Façade

The facade in the building has a small windmill dimension known as a micro wind turbine with the longest diameter being 0.30 meters while the shortest was 0.25981 meters. Moreover, the total area of the hexagons was 0.0585 m2 as indicated in Figure 7A. The "Savonius" Windmill was selected based on the consideration that it is the simplest method and works based on the differences in shear force or differential drag windmill as shown in Figures 7B and C.
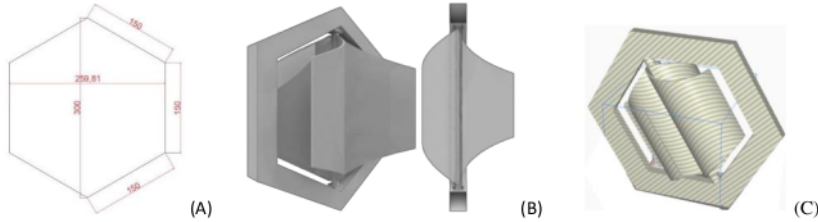

(A)   (B)   (C)

Fig. 7. (A) Dimension of Honeycomb Windmill module,
(B) Previous Design of Savonius Wind Turbine model, and (C) Optimized Savonius Wind Turbine Module with 4 Blades

3.2. Basic Theory for the Wind Turbine

Turbines are devices used in converting kinetic energy from the wind into motion energy. The amount of energy or turbine power (P) can theoretically be written as follows:

$$P = T\omega \qquad (1)$$

Where:
P = Turbine power ($watt$).
T = Torque or moment of the turbine (Nm).
ω = Angular velocity of the turbine (rad/s).

The area passed by the air was designed to have the same boundary end to the end and used as a reference value in the ANSYS Fluent 12.0 to determine the moment coefficient. Meanwhile, the dimensionless moment coefficient in line with Rahman et al. (2018, 13) is, therefore, stated as follows:

$$C_m = \frac{T}{\frac{1}{4}\rho ADV^2} \qquad (2)$$

Where:

5

C_m = Moment coefficient.
ρ = Fluid density (kg/m³).
A = Turbine blade cross-sectional area (m^2).
D = Diameter of the turbine (m).
V = Fluid velocity (m/s).

The aerodynamics in turbines also consist of several forces known as dimensionless forces such as the density and speed of the freestream body. The relationship between these two values is, however, expressed as dynamic pressure and represented using the following equation.

$$q_\infty = \frac{1}{2}\rho_\infty V_\infty{}^2 \tag{3}$$

This means it is possible to define the dimensionless force as follows:

Lift coefficient: $C_L = \frac{L}{q_\infty S}$

Drag coefficient: $C_D = \frac{D}{q_\infty S}$

Normal force coefficient: $C_N = \frac{N}{q_\infty S}$

Axial force coefficient: $C_A = \frac{A}{q_\infty S}$

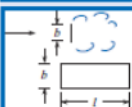Where:
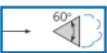L = Lifting force (N)
D = Drag force (N)
N = Normal force (N)
A = Axial force (N)
S = Extensive reference area (m^2)

The S or reference area in the coefficient was selected based on the shape of the body geometry and the values for different shapes are presented in Table 1.

Table 1. Cd values for different body shapes

	Type of Body	Length Ratio	Re	C_D
	Rectangular plate	$l/b = 1$ $l/b = 5$ $l/b = 10$ $l/b = 20$ $l/b = \infty$	$>10^4$ $>10^4$ $>10^4$ $>10^4$ $>10^4$	1.18 1.20 1.30 1.50 1.98
	Circular cylinder with axis parallel to flow	$l/d = 0$ (disk) $l/d = 0.5$ $l/d = 1$ $l/d = 2$ $l/d = 4$ $l/d = 8$	$>10^4$ $>10^4$ $>10^4$ $>10^4$ $>10^4$ $>10^4$	1.17 1.15 0.90 0.85 0.87 0.99
	Square rod	∞	$>10^4$	2.00
	Square rod	∞	$>10^4$	1.50
	Triangular cylinder	∞	$>10^4$	1.39
	Semicircular shell	∞	$>10^4$	1.20
	Semicircular shell	∞	$>10^4$	2.30
	Hemispherical shell		$>10^4$	0.39
	Hemispherical shell		$>10^4$	1.40
	Cube		$>10^4$	1.10
	Cube		$>10^4$	0.81
	Cone—60° vertex		$>10^4$	0.49
	Parachute		$\approx 3 \times 10^7$	1.20

(Source: Elger et al., 2015, 371–372)

It is possible to capture some of the kinetic energy passing through the turbine cross-section and this is expressed as the power coefficient (Cp) which can be calculated using the following formula:

$$C_p = \frac{P}{\frac{1}{2}\rho ADV^3} = \frac{T\omega}{\frac{1}{2}\rho ADV^3} = \lambda C_m \qquad (4)$$

Where:

C_p = power coefficient

P = power of the turbine (Watt).

The power coefficient of this turbine, however, depends on the Tip-Speed Ratio (TSR) which is the ratio of blade speed at the tip to the speed of airflow as indicated in the following relationship:

$$\lambda = \frac{\omega R}{V} \tag{5}$$

Where:

λ = Tip-speed ratio

R = Turbin radius (m)

The theoretical power coefficient limit is 0.59 and this is known as the Betz Limit. Meanwhile, Figure 8 shows the maximum value of the power coefficient (C_p) against TSR for different types of turbines (Kumar & Saini, 2016, 293)
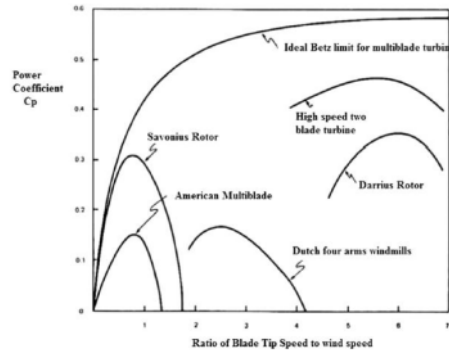

Figure 8. Power Coefficient against TSR

3.3. Simulation Validation

The validation process was conducted using a 3D model in accordance with Ferrari et al. and this involved the Savonius turbine model being in line with the Rotor C geometry [Ferrari, 2017]. Moreover, the Reynolds number used was based on turbine diameter (Dt) and bulk velocity (U$_{inf}$) which was 4.32 .105 while the wind tunnel was in line with the method applied by Blackwell et al., and the 1.4% Turbulence Intensity used was in accordance with 1% recommended by Suchde et al. (2017, 255). The two simulations conducted with the experimental results of Blackwell et. al. 1977 in the wind tunnel showed that the most optimal Savonius turbine was found at approximately TSR 0.85 with a maximum Coefficient of power (Cp) value of 0.25 as indicated in Figure 9. The other TSR variables used based on the angular velocity of the rotor turbine include 0.576, 0.804, and 1.002 while the coefficient of power value was used for comparison. Moreover, the experimental trend of the Savonius turbine performance was presented through the simulation conducted using Ansys Fluent 16.0 with 3D Dimensional, Double Precision, Pressure-Based Solver, Steady-State Condition, and Criteria Convergency 10-5. The Cell Zone conditions were also divided

8

into static and dynamic frames with the dynamic conditions specifically having the frames of motion with rotational 23 city. The simulation results of hexagonal micro wind turbine were compared with the Ferrari et al. findings and this study was discovered to have a smaller Cp due to its use of a mathematical model approach which led to some flow phenomena such as the turbulent flow which was observed to have been developing continually up to the present moment. Sutrisno et al. (2015) reported turbulence intensity as an energy reserve being converted gradually to flow and this means the flow with high turbulence tends to have stronger energy. Meanwhile, another flow phenomenon known as the swirl flow was reported by Simanjuntak et al. (2019) to have the capability to be used as a major factor in the coal drying process due to its ability to separate steam vapor in soil coal. The Savonius turbine simulation, however, used very strong turbulence and swirl flow phenomena, thereby, causing high uncertainty.
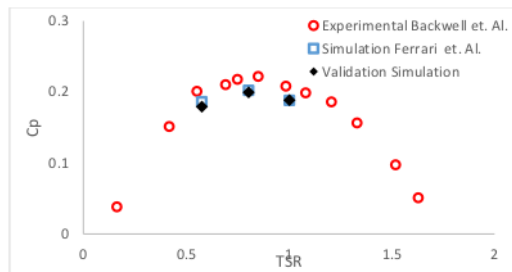

Figure 9. Comparison between the simulation results of Hexagonal micro wind turbine to Ferrari et al. and Blackwell et al.

The validation results of hexagonal micro wind turbine showed large error values of 10.45%, 10.02%, and 9.43% at TSR 0.576, 0.804, 1.002 respectively as presented in Table 2. This means the model was unable to produce better predictions than Ferrari et al.'s prediction of the experimental results of Blackwell et al due to its use of a steady-state condition. It was, therefore, recommended that the unsteady state simulation approach which requires resource computation with high-performance equipment be used in further studies. Meanwhile, some other parameters were selected for the next process which involved optimizing the hexagonal turbine design. This validation method only compares one parameter due to the focus of this study on the optimization of a new design for the Savonius turbine shape.

Table 2. Comparison of the simulation validation result with the experiment of the Blackwell et al. (1977).

TSR	Simulation Validation	Error % Cp with Experiment Blackwell et al.
0.576	0.1791	10.45
0.804	0.1994	10.02
1.002	0.1883	9.43

4. RESULTS and DISCUSSION

The software used for simulation was ANSYS FLUENT 16.0 using the following parameters:
Viscous model: RNG k-epsilon, Standard Wall Function.
Rotational velocity: varied to obtain a different TSR
Velocity inlet   : 4 m/s
Turbulent method: Intensity and length scale
Turbulent length scale: 0.001 m
Turbulent intensity   : 5 % depend on wind tunnel
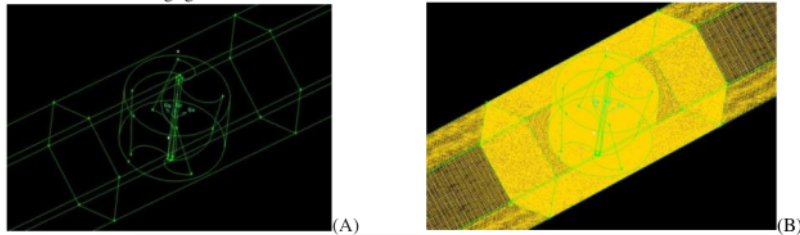3D model & meshing: gambit software

Figure 10. (A) Savonius 3D facet 3D model and (B) Savonius 3D meshing model

There is a variation in the radius, of 22, and twist of the hexagonal or honeycomb wind turbine blades used. The simulation was conducted to obtain the 18 e of the Power Coefficient for the Savonius hexagonal wind turbine using 6 radii which include 57.5 16, 58 mm, 60 mm, 64 mm, 72 mm, and 87.4 mm as showed in Figure 11A, 5 offsets including 0 mm, 5 mm, 7 mm, 9 mm, and 11 mm as indicated in Figure 11B, and the 5 twist models including 0°, 30°, 45°, 60°, and 90° as presented in Figure 11C. The design was simulated until the results converge. Moreover, a Y + check was also performed and the value was discovered not to exceed 500 (Tahani et al., 2016, 464) while flux conservation at the inlet and outlet also produced values below 1% and these were considered to be good (Suchde et al., 2017, 255).
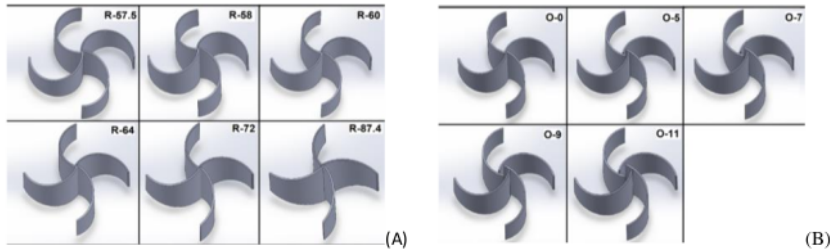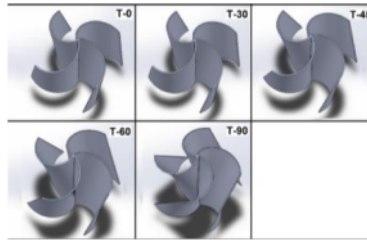
Figure 11. (A) Variation in the radius of the turbines, (B) Variation in Offset of the turbines, and (C)Variations in Twist of the turbines

Table 2 and Figures 12A and B showed the optimal value of the turbine blade was found at 58 mm radius with 0.5 TSR which produced 2.84 watts of power and torque of 0.099 Nm as indicated in Table 3 while the power coefficient (Cp) was 0.2786. The model of flow and turbulence kinetic energy produced are presented in 11A and B.
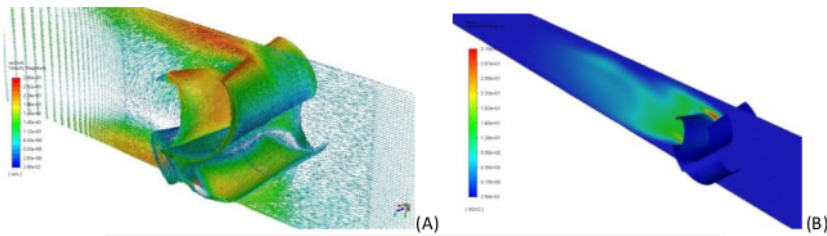

Figure 12. (A) Vector velocity of wind flow on a 58 mm radius turbine and (B) turbulent kinetic energy in a 58 mm radius turbine
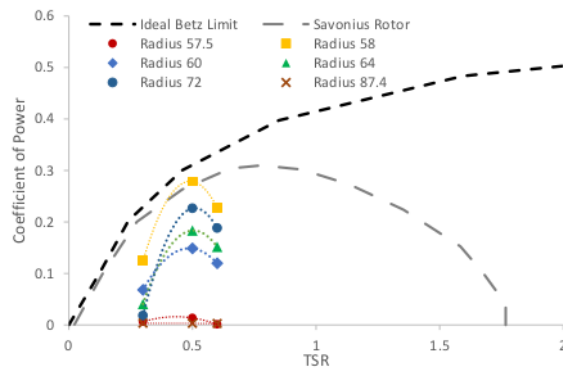

Figure 13. Variants of Turbine Blade Radius

11

Figure 13 shows the three models with 58 mm, 64 mm, and 72 mm radius, and the highest C_P values have the same flow velocity patterns. It was also discovered that a smaller drag flow was produced when the radius was fixed and this is less favorable for the performance of the turbine. Moreover, a larger radius produced a larger counter-rotating-vortices flow which is also less favorable for performance due to its smaller overlap flow. However, the greatest turbulent kinetic energy distribution in the rotor was found in turbines with the smallest diameter which was 58 mm. This means a larger diameter of the rotor produced the smaller distribution of turbulent kinetic energy as presented in Figure 12B.

Table 3. Variations in Turbine Blade Radius

Radius (mm)	TSR	C_P	Power (Watt)	Torque (N.m)	Y Plus
	0.3	0.0063	0.01414182	0.001355268	83.13049
57.5	0.5	0.01362	0.138701848	0.004817709	132.4085
	0.6	0.00102	0.006001218	0.000208448	112.7113
	0.3	0.12423	0.278864743	0.026724749	85.26819
58	0.5	0.2786	2.837076273	0.098543809	132.8681
	0.6	0.22797	1.338171874	0.04648044	112.3835
	0.3	0.06798	0.152605393	0.014624799	88.38058
60	0.5	0.14847	1.511890424	0.052514429	134.181
	0.6	0.11964	0.702281366	0.02439324	113.8718
	0.3	0.04071	0.091376894	0.008757022	94.81096
64	0.5	0.18333	1.866906431	0.064845656	144.2127
	0.6	0.15165	0.890188959	0.030920075	122.4319
	0.3	0.01791	0.040192929	0.003851853	102.9334
72	0.5	0.22628	2.304257532	0.080036733	156.9534
	0.6	0.18799	1.10346569	0.038328089	133.3397
	0.3	0.00319	0.007153723	0.000685571	111.8106
87.4	0.5	0.00312	0.031819299	0.001105221	184.3163
	0.6	0.00266	0.015604645	0.000542016	156.7907

Table 4 and Figures 14A and B show the optimal value of the turbine blade was produced at 11 mm offset with 0.5 TSR as indicated by the production of 3.05 watts of power, 0.106 Nm of torque, and 0.29918 power coefficient (C_P). The model of flow and turbulence kinetic energy produced are presented in Figure 13B.
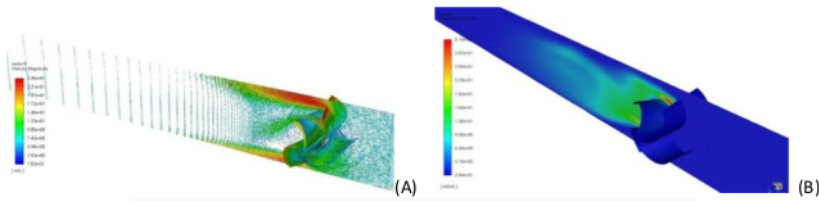

(A)   (B)

Figure 14. (A) Vector velocity of wind flow on an 11 mm offset turbine, and (B) turbulent kinetic energy in turbine offset 11 mm
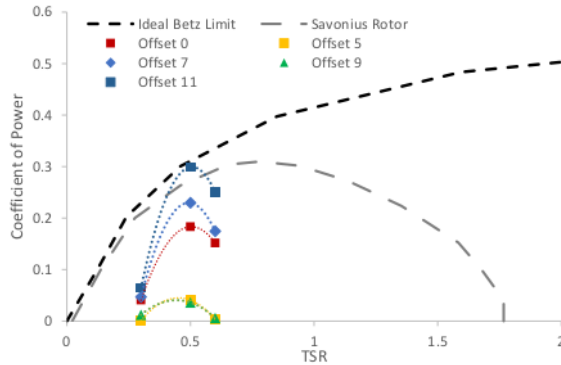
12

Figure 15. Variants of Turbine Blade Offset (Source: Author)

Figures 15 showed the three models with 11, 7, and 0 offsets with the highest C_P values have almost the same flow velocity patterns. A smaller drag flow was produced when the offset was reduced and this is less favorable to the performance of the turbine and the same was also observed for smaller offsets which caused a greater counter-rotating-vortices flow and smaller overlap flow. Meanwhile, the greater offset of the rotor was observed to cause smaller distribution of turbulent kinetic energy before it increased again.

Table 4. Variations in Turbine Blade Offset

Offset (mm)	TSR	C_P	Power (Watt)	Torque (N.m)	Y Plus
	0.3	0.04071	0.091377	0.008757	94.81096
0	0.5	0.18333	1.866906	0.064846	144.2127
	0.6	0.15165	0.890189	0.03092	122.4319
	0.3	0.00095	0.002122	0.000203	87.08589
5	0.5	0.04072	0.414702	0.014404	132.0764
	0.6	0.00335	0.019688	0.000684	112.0743
	0.3	0.04683	0.105127	0.010075	84.6218
7	0.5	0.22955	2.337588	0.081194	128.1884
	0.6	0.17445	1.023987	0.035567	108.7234
	0.3	0.01217	0.027321	0.002618	82.36165
9	0.5	0.03606	0.367162	0.012753	124.5991
	0.6	0.00611	0.035872	0.001246	105.5825
	0.3	0.06421	0.144118	0.013811	80.24362
11	0.5	0.29918	3.046607	0.105822	121.2431
	0.6	0.250932	1.472946	0.051162	102.7176

Table 4 and Figure 16 show that the optimal value of the turbine blade was at 0-degree twist with 0.5 TSR which produced 4.75 watts of power, 0.165 Nm of torque, and 0.4665 of power coefficient. The model of the flow and turbulence kinetic energy produced is presented in Figure 16B.
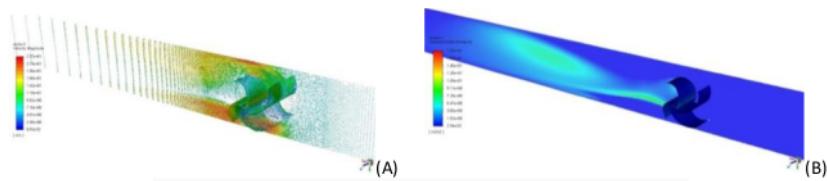
Figure 16. (A)Vector speed of wind flow on turbine twist 0º and (B) turbulent kinetic energy in turbine twist 0º
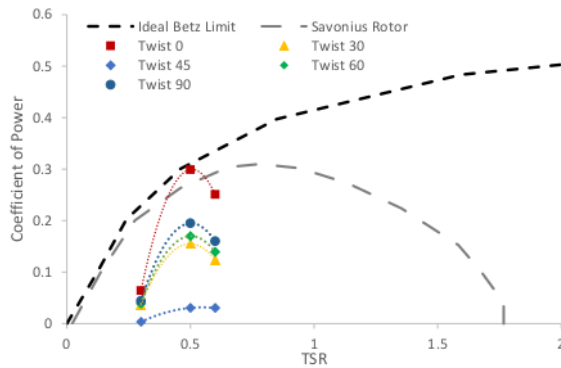

Figure 17. Variants of Turbine Blade Twist

Figure 17 shows the three models 0, 90, and 60 twists with the highest C_P values have almost the same flow velocity patterns. It was discovered that the minimized twist produced a smaller drag flow, and this is less favorable for the performance of the turbine due to its larger counter-rotating-vortices flow. A bigger twist also caused smaller overlap flow which is also considered less favorable and this means a greater twist of the rotor usually leads to a higher distribution of turbulent kinetic energy before the distribution shrinks again.

Table 5. Variations in Turbine Blade Twist

Twist (degree)	TSR	C_P	Power (Watt)	Torque (N.m)	Y Plus
	0.3	0.06421	0.144118	0.013811	80.24362
0	0.5	0.29918	3.046607	0.105822	121.2431
	0.6	0.250932	1.472946	0.051162	102.7176
	0.3	0.0367	0.082452702	0.00790178	73.73257
30	0.5	0.15497	1.578151371	0.054815956	113.7554
	0.6	0.12406	0.728239091	0.025294862	97.44502
	0.3	0.00339	0.007624782	0.000730714	74.97164
45	0.5	0.03044	0.309972006	0.010766655	113.4298

Twist (degree)	TSR	C$_P$	Power (Watt)	Torque (N.m)	Y Plus
	0.6	0.03041	0.178473013	0.006199132	96.20094
	0.3	0.03888	0.087283209	0.008364707	72.77678
60	0.5	0.1699	1.730730969	0.060115699	112.8925
	0.6	0.13926	0.817438314	0.028393134	97.33451
	0.3	0.0441	0.099087932	0.009496002	62.60502
90	0.5	0.1949	1.984248782	0.068921458	98.08689
	0.6	0.1599	0.938463598	0.03259686	85.9093

The simulation further combined 58 mm radius, 11 mm offset, and 0° twist and the optimal result was also recorded at TSR 0.5 as indicated by 3.046607 Watts power, 0.105822 Nm torque, and 0.29918 Power Coefficient (C$_P$) produced.

Table 6. Variations in Turbine Blade TSR

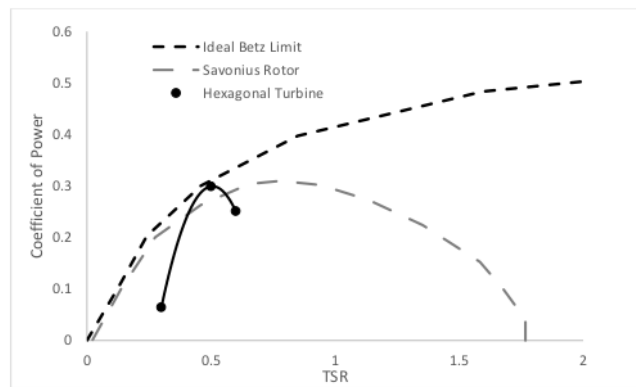| TSR	C$_P$	Power (Watt)	Torque (N.m)	Y Plus
0.3	0.06421	0.144118	0.013811	80.24362
0.5	0.29918	3.046607	0.105822	121.2431
0.6	0.25093	1.472946	0.051162	102.7176

Figure18. Hexagonal Turbine Optimum Model

5. Conclusions

Numerical and CFD simulations were used to analyze the three parts of designing and optimizing the honeycomb module of Savonius micro wind turbine with 4 blades on the second façade building using radius, twist, and offset as the important factors to determine the performance.

The use of 58 mm radius, 11 mm offset, zero-degree twist blade, and 0.5 TSR in one-piece module design of the micro hexagonal wind turbine was found to have produced 3.047 watts of electricity which eliminated the piece modules of honeycomb photovoltaics (as explained in next research) while the optimal Power of Coefficient (C_p) was 0.29918.

The comparison of the Savonius turbine with the Hexagonal Turbine at a TSR of 0.5 showed the Hexagonal Turbine has a lower TSR leading to a smaller U_{inf} requirement. This prediction is associated with the 4 blades used in the design which is more than the Savonius turbine, thereby, causing an increment in the solidity which is very important for the VAWT more than the HAWT. It is also pertinent to note that the high solidity reduces the operating rotation of the wind turbine. Moreover, the Cp value of the Hexagonal Turbine was also found to be higher and close to the Betz limit which is the maximum allowed for wind turbines.

The previous design of Hexagonal Savonius with 4 blades at 90 mm radius as well as unknown offset and twist which was tested in wind tunnel produced only 0.03426 power of coefficient (C_p) and 0.12 watt of electricity. This, therefore, means the numerical and CFD simulation was successfully used to determine the optimal blade radius, offset, and twist to produce renewable energy in hexagonal micro wind turbine architectural building façade.

References

Ahmed, M.M.A., Rahman, A.K.A., Ali, A.H.H., Suzuki, M. (2016). Double Skin Façade: The State of Art on Building Energy Efficiency. *Journal of Clean Energy and Technologies, 4(*1), 84-89.

Arteaga-López, E., Ángeles-Camacho, C., & Bañuelos-Ruedas, F. (2019). Advanced methodology for feasibility studies on building-mounted wind turbines installation in urban environment: Applying CFD analysis. *Energy, 167*, 181–188. https://doi.org/10.1016/j.energy.2018.10.191

Attoye, D.E., Adekunle, T.O., Tabet Aoul, K., & Hassan, A., (2018). Building Integrated Photovoltaic (BIPV) Adoption: A Conceptual Communication Model for Research and Market Proposals. A Conference Proceeding ASEE Connecticut, USA.

Blackwell, B., Sheldahl, R., & Feltz, L. (1977). Wind Tunnel Performance Data for Two and Three Bucket Savonius Rotors. *Journal of Energy, 2*(3), 160-164.

Cao, X.D., Xilei, D., & Liu, J. (2016). Building Energy-Consumption Status Worldwide and the State-of-the-Art Technologies for Zero-Energy Buildings during the Past Decade. *Energy and Building, 128*, 1-58.

California Energy Commission (2005). Options for Energy Efficiency in Existing Buildings.

Coyle, E.D., Grimson, W., Basu, B., Murphy, M. (2014). Understanding the Global Energy Crisis. Book Chapter part 1: *Reflection on Energy, Greenhouses Gases, and Carbonaceous Fuels*. Purdue University Press.

Daryanto, Y. (2007). *Kajian Potensi Angin untuk Pembangkit Listrik Tenaga Bayu*. Yogjakarta: BALAI PPTAGG – UPT – LAGG.

Dudley, N. (2008). Climate Change and the Energy Crisis. Back to the Energy Crisis – the Need for a Coherent Policy towards Energy Systems. *Policy Matters*, *16*, 12-68.

Elger, D.F., LeBret, B.A., Crowe, C.T., & Robertson, J.A. (2015). *Engineering Fluid Mechanics* (9th ed.).

Ferrari, G., Federici, D., Schito, P., Inzoli, F., & Mereu, R. (2017). CFD Study of Savonius Wind Turbine: 3D model Validation and Parametric Analysis. *Journal of Renewable Energy, 105,* 722-734.

Howells, M., & Roehrl, R.A. (2012). Perspective on Sustainable Energy for the 21th Century (SD21). New York: United Nations Department of Economic Social Affairs, Division for Sustainable Development.

IEA. (2004b). Energy Balances for OECD Countries and Energy Balances for Non-OECD Countries, Energy Statistics for OECD Countries and Energy Statisics for Non-OECD Countries (2004 editions), Paris.

Kumar, A., & Saini, R.P. (2016). Performance Parameter of Savonius Type Hydrokinetic Turbine: A Review. *Journal of Renewable and Sustainable Energy Reviews*, *64*, 289-310.

Manienyen, V., Thambidurai, M., and Selvakumar, R. (2009). Study on Energy Crisis and the Future of Fossil Fuels. *Proceeding of SHEE, Engineering Wing, DDE.*, Annamalai University, December 11-12, 2009.

Manwell, J.F., McGowan, J.G., & Rogers, A.L. (2010). *Wind Energy Explained: Theory, Design and Application* (2nd ed.). Wiley.

Mintorogo. D.S., Elsiana, F., & Budhiyantho, A. (2019). Experimental Sustainable Micro Wind Turbines on Second Façade of Buildings. A Research Report. Center for Research, Petra Christian University.

Nowak, D.J., Greenfield, E.J., & Ash, R.M. (2019). Annual Biomass Loss and Potential Value of Urban Tree Waste in the United States. *Urban Forestry & Urban Greening, 46*. 126469. https://www.fs.fed.us/nrs/pubs/jrnl/2019/nrs_2019_nowak_004.pdf. (June, 2020).

Park, J., Jung, H.J., Lee, S.W., Park, J. (2015). A new Building-Integrated Wind Turbine System Utilizing the Building. *Energies*, *8*, 11846–11870.

Rahman, M., Salyers, T.E., El-Shahat, A., Ilie, M., Ahmed, M., & Soloiu, V. (2018). Numerical and Experimental Investigation of Aerodynamic Performance of Vertical-Axis Wind Turbine Models with Various Blade Designs. *Journal of Power and Energy Engineering*, *6*(5), 13-14. https://doi.org/10.4236/jpee.2018.65003

Suchde, P., Kuhnert, J., Schröder, S., & Klar, A. (2017). A flux conserving meshfree method for conservation laws. *International Journal for Numerical Methods in Engineering, 112*(3), 238–256. https://doi.org/10.1002/nme.5511

Sutrisno, Mirmanto, H., Sasongko, H., Noor, D. Z. (2015). Study of The Secondary Flow Structure Caused the Additional Forward-facing Step Turbulence Generator. *Advances and Applications in Fluid Mechanics* 18(1), 129-144. http://dx.doi.org/10.17654/AAFMJul2015_129_144

Simanjuntak, M. E., Prabowo, Widodo, W. A., Sutrisno, Sitorus, M. B. H. (2019). Experimental and Numerical Study of Coal Swirls Fluidized Bed Drying on 10° Angle of Guide Vane. *Journal of Mechanical Science and Technology,* 33, 5499-5505.

https://doi.org/10.1007/s12206-019-1042-2.

Tahani, M., Babayan, N., Mehrnia, S., & Shadmehri, M. (2016). A Novel Heuristic Method for Optimization of Straight Blade Vertical Wind Turbine. *Energy Conversion and Management*, *127*, 461–476. https://doi.org/10.1016/j.enconman.2016.08.094

Wenehenubun, F., Saputra, A., & Sutanto, H. (2015). An experimental study on the performance of Savonius wind turbines related with the number of blades. *Energy Procedia*, *68*, 297–304. https://doi.org/10.1016/j.egypro.2015.03.259

Harvesting Renewable Energies through Innovative Kinetic Honeycomb Architectural Facades: The Mathematical & CFD Modeling for Wind Turbine Design Optimization

"Experimental validation of the age-of-the-air CFD analysis: A case study", Science and Technology for the Built Environment, 2018
Publication

6   Nauman Riyaz Maldar, Cheng Yee Ng, Elif Oguz. "A review of the optimization studies for Savonius turbine considering hydrokinetic applications", Energy Conversion and Management, 2020
Publication   <1 %

7   docplayer.net
Internet Source   <1 %

8   www.supremecourt.gov
Internet Source   <1 %

9   Majid Eshagh Nimvari, Hossein Fatahian, Esmaeel Fatahian. "Performance improvement of a Savonius vertical axis wind turbine using a porous deflector", Energy Conversion and Management, 2020
Publication   <1 %

10 S Suriadi, W I Daru, S R Halid, M Syukri, M Gapy. "The optimization of hybrid power generator system (PV-Wind turbine) using Homer software", IOP Conference Series: Materials Science and Engineering, 2021
Publication   <1 %

11 hdl.handle.net
Internet Source

<1 %

12 Submitted to Chapman University
Student Paper   <1 %

13 Illa Rizianiza, S Devy Setiorini, Alfian Djafar.
"The Effect of The Angle of Attack of the
Electric Power Generated on Prototype of the
Horizontal Axis Wind Turbine", IOP
Conference Series: Materials Science and
Engineering, 2019
Publication   <1 %

14 Ridwan, I Setyawan, Setiyono. "Performance
of vertical axis Savonius wind turbines related
to the fin number on the blade", IOP
Conference Series: Materials Science and
Engineering, 2019
Publication   <1 %

15 eprints.uthm.edu.my
Internet Source   <1 %

16 ia801304.us.archive.org
Internet Source   <1 %

17 journals.sagepub.com
Internet Source   <1 %

18 spb-stream.ru
Internet Source   <1 %

www.scirp.org

19   Internet Source   <1%

20   C M Shashikumar, Hindasageri Vijaykumar, Madav Vasudeva. "Numerical investigation of conventional and tapered Savonius hydrokinetic turbines for low-velocity hydropower application in an irrigation channel", Sustainable Energy Technologies and Assessments, 2021   <1%
Publication

21   Lee, Jae Seong, Juhyeong Seo, Ho Young Kim, Jin Taek Chung, and Sam S. Yoon. "Effects of combustion parameters on reforming performance of a steam–methane reformer", Fuel, 2013.   <1%
Publication

22   Vimal Patel, T.I. Eldho, S.V. Prabhu. "Velocity and performance correction methodology for hydrokinetic turbines experimented with different geometry of the channel", Renewable Energy, 2018   <1%
Publication

23   Wenhao Xu, Gaohua Li, Xiaobo Zheng, Ye Li, Shoutu Li, Chen Zhang, Fuxin Wang. "High-resolution numerical simulation of the performance of vertical axis wind turbines in urban area: Part I, wind turbines on the side of single building", Renewable Energy, 2021   <1%

| 24 | betterplan.squarespace.com
Internet Source | <1 % |

| 25 | iieta.org
Internet Source | <1 % |

| 26 | mts.intechopen.com
Internet Source | <1 % |

| 27 | s3-eu-west-1.amazonaws.com
Internet Source | <1 % |

| 28 | Jeongsu Park, Hyung-Jo Jung, Seung-Woo Lee, Jiyoung Park. "A New Building-Integrated Wind Turbine System Utilizing the Building", Energies, 2015
Publication | <1 % |

| 29 | T. Stathopoulos, H. Alrawashdeh. "Chapter 1 Urban Wind Energy: A Wind Engineering and Wind Energy Cross-Roads", Springer Science and Business Media LLC, 2019
Publication | <1 % |

Exclude quotes   On   Exclude matches   Off
Exclude bibliography   On